University of BRISTOL

Mitsubishi L200 Solar Panel Deployment Platform Technical Analysis Report

Abdullah Monnoo (ul21823), Ibrahim Arekat (wq21745), Kabeer Dayal (pb21912), Ein Lertnawapan (fm21936)

Group 7

Report Date: 04/05/2023

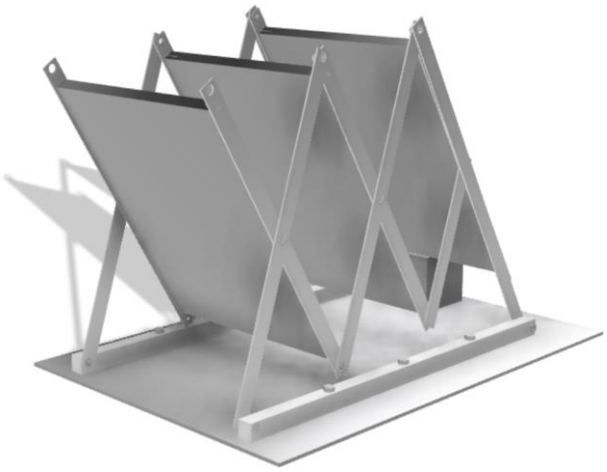

1.0 Initial Model

An analysis of the system was based on using inverted pendulum model as shown in Figure 1. The model was based on the assumptions shown in Table 1.

Table 1: Assumptions and Effects

Assumption	Effect
MOI (Moment of Inertia) based on a point mass distance along a bar	MOI may differ based on distribution of mass relative to pivot
Friction Negligible	Since the system was slow, friction had little effect
Distance of centre of mass from pivot changes linearly with relation to angle	Relationship may not be linear
The true rotating bars were assumed to be at the same angle as the pendulum bar	This would affect the true torque required and damping.
No energy used in changing radius i.e., system force is purely rotational.	In real system, energy will used to extend
Drag is constant when considered	The true drag would be a function of $\boldsymbol{\theta}$, and would likely increase with deployment
Coefficient of drag = 1	Coefficient is probably lesser

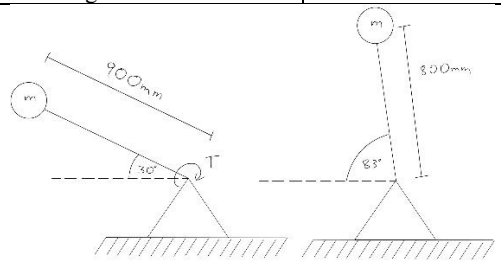

Figure 1: Inverted Pendulum Initial and Final State

First the $\boldsymbol{\theta_0}$, $\boldsymbol{\theta_1}$, $\boldsymbol{r_0}$, $\boldsymbol{r_1}$, were measured via the CAD model by using Fusion 360's COM function in the fully deployed and undeployed positions and measuring the distance between the main pivot and the COM. These were used to develop a linear relationship between $\boldsymbol{\theta}$ and $\boldsymbol{r}$ as in Equation [1].

$$r(\theta) = \left(\frac{r_1 - r_0}{\theta_1 - \theta_0}\right) \cdot \theta + r(0) \quad [1]$$

MOI was found as that for the point mass of a pendulum in Equation [2].

$$I = m \cdot (r(\theta))^2 \quad [2]$$

These were used with the 2nd Order ODE [3].

$$\alpha = \frac{\tau(\omega) - \sum \tau_{res}}{I} \quad [3]$$

$$\tau(\omega) = \left(\tau_{stall} - \left(\frac{\tau_{stall}}{\omega_{no\ load}}\right) \cdot \omega\right) \cdot G_r \cdot \eta \quad [4]$$

$$\sum \tau_{res} = (m \cdot g \cdot \cos\theta + F_{drag} \cdot \sin\theta) \cdot r(\theta) + d_\tau(\omega, \theta) \quad [5]$$

Initially, Gearbox efficiency was assumed to be 100%, and drag force as well as the damping coefficient to be 0N. Under these assumptions, using the 4th order Runge-Katta numerical method was used on python to solve the equation [3] while using a step size of 0.001s. Equation [6] was used to calculate power output, and Equation [7] for input.

$$P_{out} = \left(\tau \cdot \omega - \left(\frac{\tau_{stall}}{\omega_{no\ load}}\right) \cdot \omega^2\right) \cdot \eta \quad [6]$$

$$P_{in} = V \cdot \left(\left(\tau_{stall} - \left(\frac{\tau_{stall}}{\omega_{no\ load}}\right) \cdot \omega\right) \cdot \left(\frac{\tau_{stall}}{i_{no\ load}}\right) + i_{no\ load}\right) \quad [7]$$

Integrating power with respect to time, a total efficiency was found against gear ratio. Time and efficiency were plotted against gear ratios in the figures starting from just above the holding ratio up till 2.5x the holding ratio.

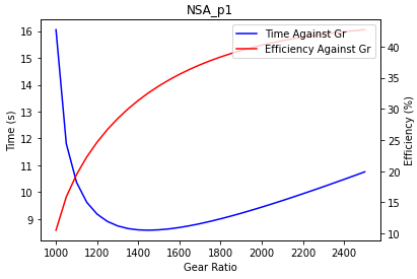

Figure 2: NSA_p1 Time and Efficiency vs GR

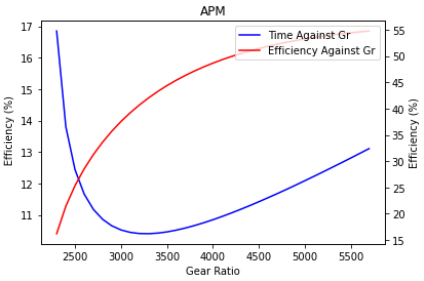

Figure 3: APM Time and Efficiency vs GR

As shown in the figures 2,3,4 and 5, all motors achieved a similar efficiency of about 35% except for APM, achieving around 50%. NSA-I P3 had the fastest deployment time of 2.6s while NSA-I p2 followed with 4 seconds under a similar efficiency. NSA-I P1and APM had slower deployment times and required high gear ratios so they were omitted from consideration.

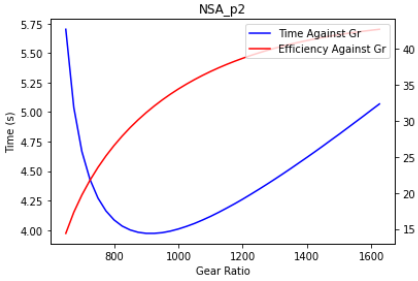

Figure 4: NSA_p2 Time and Efficiency vs GR

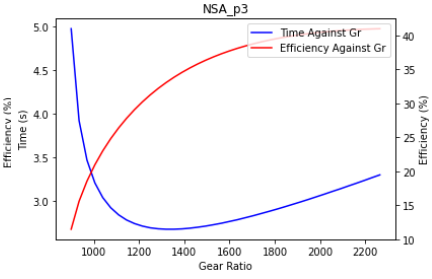

Figure 5: NSA_p3 Time and Efficiency vs GR

From these graphs, a general idea of the required gear ratios was achieved.

2.0 Final Model and Further Analysis

After decreasing the selection of candidate motors, deeper analysis of specific gear ratios and efficiencies could be done. Since a worm gear was expected to be used to achieve these high ratios alongside spurs, gearbox efficiency (η) was assumed to be constant at 50% across all models. Final selection between the motors was achieved through simulating with aerodynamic loads and damping for deployment as well as retraction. As per requirement 6, the mechanism must be operable under winds of up to 32km/h. Aerodynamic Load at this windspeed was calculated to be 90N and modelled to act at the COM against the direction of deployment parallel to the ground. Using the ratio for the fastest deployment of each gear, the retraction of the system was modelled with the winds of 90N acting with the system on the COM point. Since it was known that the system could act against the wind load, this was modelled to ensure the system operated normally at safe speeds when wind was acting alongside it. Figures 6 and 7 show the values from the final model.

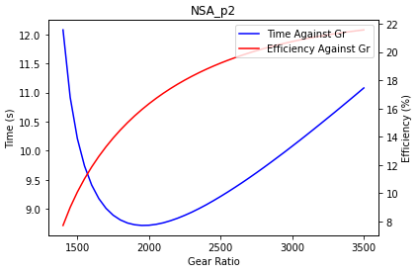

Figure 6: NSA_p2 Time and Efficiency vs GR

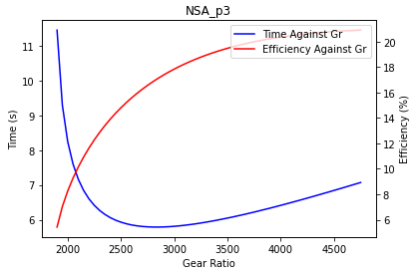

Figure 7: NSA_p3 Time and Efficiency vs GR

For the retraction, modified equations had to be used. For most of the deployment the motor would be above the no load speed, so the gearbox efficiency term would be multiplied with the $\sum\tau_{res}$ term rather than the motors driving torque $\tau(\omega)$.

$$\tau(\omega) = \left(\tau_{stall} - \left(\frac{\tau_{stall}}{\omega_{no\ load}}\right) \cdot \omega\right) \cdot G_r \quad [8]$$

$$\sum\tau_{res} = ((m \cdot g \cdot \cos\theta + F_{drag} \cdot \sin\theta) \cdot r(\theta) + d_\tau(\omega, \theta)) \cdot \eta \quad [9]$$

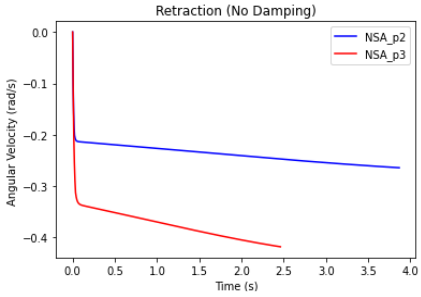

Figure 8: Angular Velocity Retraction(No Damping)

Linear Dampers were added to determine if they influenced the safety of the system in relevance to requirement 14. Figure 8 shows velocities with no damping. After manual runs of the model, a way to fix a pair of linear dampers was found which approximately achieved the maximum stroke length of the damper, thus creating the greatest effect. Thus, the linear damper was fixed to the mounting bar 0.3 (a) metres from the motor, and on the deployment bar 0.1 (b) metres from the motor. The damping coefficient d_c was set as 54000Ns/m and damping was modelled by equations [10].

$$d_\tau(\omega,\theta) = \frac{d_c \cdot a^2 \cdot b^2 \cdot \omega \cdot \sin^2\theta}{d_{Length}(\theta)} \qquad [10]$$

$$d_{Length}(\theta) = \sqrt{a^2 + b^2 - 2 \cdot a \cdot b \cdot \cos\theta} \qquad [11]$$

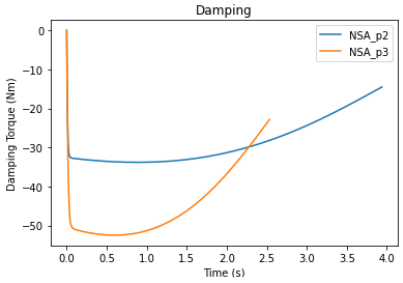

Figure 9: Damping Torque Against Time

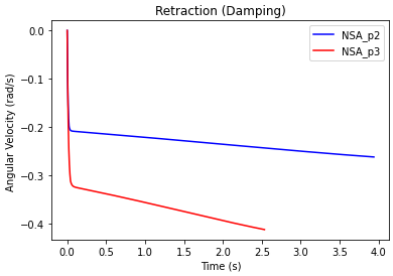

Figure 10: Angular Velocity Retraction (Damping)

As shown in figure 10, damping(figure 9) hardly had a noticeable difference except decreasing the times by approximately 0.1s. It should be noted that the motor was acting as a rotational damper, further described in the motor selection in the design report. The motor characteristic curve was then extrapolated to calculate the voltage past the no load speed via equation [12].

$$V = \frac{\omega}{\left(\frac{\tau_{stall}}{i_{no\ load}}\right)} - 2 \cdot i_{no\ load} \qquad [12]$$

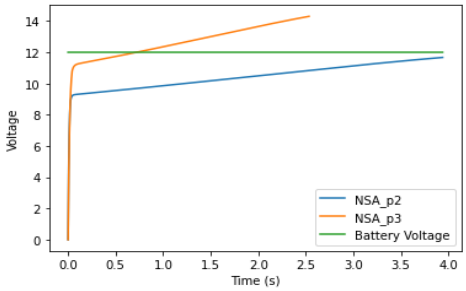

Figure 11: Voltage across motor against Time

As seen in figure 11, the NSA-I P3 would exceed the voltage supply of the battery creating a back voltage of 14V at its peak. The NSA-I P2 however would just stay below the 12V supplied by the battery. A back voltage would force countermeasures to be added against damage to the circuit. In conclusion, lower gear ratio, no back voltage and fast deployment time favoured the motor NSA-I P2.